

TRICKLE BEDS

I-14. Catalytic Wet Air Oxidation of Phenol in Packed-Bed Reactors Over Pillared Clay Catalyst

A. Problem Definition

Diversity of wastewater generated from petroleum, chemical agricultural, pulp and paper, and other process industries contains organic pollutants in the range of a few hundred to a few thousand ppm. These wastes are too dilute to incinerate, yet too toxic to be biologically treated. Among the possible processes for aqueous wastewater treatment the solid-catalyzed wet oxidation (CWO) using air is promising for achieving high conversion of the organic pollutants. However, the current typical process conditions are high pressure (5-15 MPa) and high temperature (200-325°C). Further improvement of catalyst performance, however, is needed for wider use of the wet oxidation process. If a catalyst can be developed that works effectively below 150 °C, catalytic wet oxidation would be a potential process for more general water treatment (Imamura, 1999). Up to now several newly developed catalysts were proposed in order to reduce the severity of the reaction conditions. Among the promising materials, Al-Fe pillared clay catalyst has shown encouraging results for oxidizing organic compounds in aqueous media in different reactors, including slurry reactor and basket stirred tank reactor. This novel catalyst allows for mild conditions and can be used for a rather long time with stable performance. Therefore, the Al-Fe pillared clay catalyst is going to be employed in this work in order to further explore its potential.

B. Research Objectives

1. Evaluate the performance of the bench-scale packed bed (upflow and downflow) using the pillared clay catalyst for phenol oxidation in aqueous solution and optimize operating conditions.
2. Characterize the fresh and spent catalysts to study the catalyst stability and long-term activity.

C. Research Accomplishments

An experimental study for comparing the behavior of a packed bed reactor in the catalytic liquid-phase oxidation of aqueous phenol with two modes of operation, downflow and upflow, has been presented. The operating parameters investigated included temperature, reactor pressure, gas flowrate, LHSV, and feed concentration. The reaction was found to be liquid-limited at high pressure and low phenol feed concentrations, but it approached gas-limited at low pressure and high feed concentrations of phenol. It was shown that the upflow reactor generally performs better when the liquid reactant limitation controls the rate, because of the completely wetted catalyst. The interaction between the reactor hydrodynamics, mass transfer and reaction kinetics was discussed. The complete phenol removal and significant total organic carbon (TOC) reduction can be achieved at rather mild conditions of temperature (150-170°C) and total pressure (1.5-3.2 MPa) for both operation modes. The results show that the phenol and TOC conversion are considerably affected by the temperature, while the air pressure only has minor influence. The developed CWO process was used to treat a rather high phenol concentration (2000 ppm) over the Al-Fe

pillared clay catalysts. The results showed significant phenol abatement (92%) and high TOC reduction (89%). Complete elimination of TOC proved to be difficult since acetic acid, as the main intermediate, are resistant to the catalytic wet oxidation.

Various characterization methods were employed for fresh and aged pillared clay catalysts previously used in packed-bed operation. The nitrogen adsorption for the catalysts revealed the presence of a large number of micropores and mesopores. Surface analysis showed that the incorporated Al and Fe species were homogeneously dispersed between the silicate layers. During the packed-bed operation, leaf-like carbon deposits were found to build up on the catalyst active sites, and trace amounts of Fe and Al were detected in the liquid effluent, precluding a leaching type of deactivation. The Al-Fe pillared clay catalyst exhibited a fairly stable phenol conversion rate over a long period at elevated temperature and pressure (170 °C, 3.2 MPa). Therefore, the catalytic oxidation process is suitable for treatment of wastewaters containing phenol.

D. Future Work

- 1) Conduct further experiments on the two modes of operation in packed-bed reactors to generalize the conclusions obtained from this study for phenol removal.
- 2) Compare the simulation based on the developed packed bed model with the experimental observations.

For additional information, please contact Jing Guo at CREL at jingguo@che.wustl.edu, (314)-9354729.

E. References and Supplemental Information

1. Imamura S. Reviews: Catalytic and Noncatalytic Wet Oxidation. *Ind. Eng. Chem. Res.* **1999**, 38, 1743.

I-15. Experimental and CFD Study of the Liquid Flow Distribution in Trickle Bed Reactors

A. Problem Definition

Trickle Bed Reactors (TBR) are used in many petroleum and petrochemical processes like hydrotreating, hydrocracking, hydrodesulfurisation, etc.

In many industrial processes very high reactant conversion is required, like for instance in the process of reducing the sulfur content of gas oils because of an extreme constraint on sulfur content demanded by the law (50 ppm in Europe in 2005). However the catalyst packing, where the reaction takes place, is generally not optimally used in trickle bed reactors.

B. Research Objectives

Trickle bed reactors performance could be significantly increased if a proper gas and liquid distribution is achieved over the packing. Hence this study aims at contributing to a better fundamental understanding of 3-phase trickle flow distribution and its prediction.

First objective is to increase the database of experimental results in trickle flow condition for various designs of distributor for the TBR and various operating conditions.

Second objective is to implement and test Computational Fluid Dynamics codes within the framework of Fluent to predict liquid flow in TBRs.

C. Research Accomplishments

The work carried out so far as been focused on the experimental part. The CFD modeling part is currently in progress.

C.1. Measurement methods

First, with the help of a specially designed collector tray divided in $N = 25$ sectors, exit liquid fluxes at the bottom of the column were measured and the liquid distribution was investigated. Liquid distribution was assessed with the experimental data using the Maldistribution factor, Mf , defined as follows:

$$Mf = \sqrt{\frac{1}{N(N-1)} \sum \left(\frac{F_n - \bar{F}}{\bar{F}} \right)^2}$$

where F_n is the liquid flux in the sector n and \bar{F} is the averaged flux over the cross-section.

Second, the computed tomography (CT) was used as a non-invasive technique to measure the local liquid saturation in cross sections of the column. By moving up and down the CT setup

along the column. Further details about the hardware, software, and the scanning procedure have been described by Kumar et al. (1995 and 1997) and Chen et al. (2001).

C2. Experimental work

First, experimental investigations of the gas-liquid distribution at various conditions in the trickle flow regime were conducted using a central point liquid inlet centered at the top of the bed. The effects of the following parameters on the liquid distribution were investigated: liquid superficial velocity (U_L), gas superficial velocity (U_G), and packing bed height.

Two different measurements were done: with an initially dry bed and with a pre-wetted bed. In both cases, liquid jet gets wide from the top of the bed and then slowly spreads radially. This very high spreading in the first centimeters of the bed is due to the high liquid pressure generated when liquid impacts the narrow catalyst bed.

For a single tube as water inlet, the effect of liquid and gas superficial velocities on liquid maldistribution can be summarized as follows: increasing U_L decreases maldistribution, whereas increasing U_G increases maldistribution and decreases the effect of U_L . In addition, increasing the packed bed height increases the spreading of the liquid jet. Also, the pre-wetting increases the liquid spreading.

Then, the same experiments were carried out with an industrial distributor as liquid inlet. With this liquid inlet the bed was always pre-wetted.

Both distributions of liquid fluxes and liquid saturation are very homogeneous.

Low effect of liquid and gas superficial velocities are noticed but the maldistribution increases a little when the gas velocity increases, and decreases in the same range when the liquid velocity increases.

Other hydrodynamics parameters such as pressure drop, liquid holdup and bed porosity were studied.

The pressure drop of the bed and the pressure drop of the collector were measured with a U-tube filled with water. Even if it generates an important pressure drop, the collector does not affect a lot the liquid distribution. This leads to the conclusion that measurements with the collector are accurate. Moreover, pressure drop is higher with pre-wetting than without, and it is also higher with the industrial distributor than with the tube as water inlet. Thus, increasing liquid or gas flows increases pressure drop.

Dynamic and static liquid holdup values, were obtained using the collector and a weighing system, are in good agreement with values found in the literature.

Both the radial and the vertical variations of porosity in the bed were determined. The porosity decreases in the first twenty centimeters of the bed and then becomes almost constant, between 0.365 and 0.37. Porosity is higher close to the wall than in the center of the

reactor. Results were compared with the ones available in the literature and are in good agreement.

C.2. CFD work

Simulations are performed in an Euler-Euler approach to simulate the gas/liquid flow in the TBR in trickle flow regime.

Previous work of Jiang et al. (2002) developed in CFDLib framework (Los Alamos National Laboratory CFD Code) is used as a basis to develop Fluent simulations. First, the statistical description of the porosity profile of the packed bed was successfully implemented. Furthermore, interactions between the three present phases were modeled on the basis of Attou's (1999, 2000) annular approach.

Simulation was also been run with CFX software from AEA Technology for comparison purposes.

C. Future Work

As far as the CFD part is concerned, consideration of the drag forces needs to be further improved. Moreover, effect of the capillarity needs to be taken into account as it reportedly has a drastic effect on the liquid flow in the porous media of the packed bed. Various approach are being investigated.

This study provides a good database for simulation of trickle bed reactors by CFD. In the short term, these results should enable to improve the actual predictions of the water flow in a trickle bed reactor. In the long term, simulation might be able to predict flow of every liquid in every kind of catalyst.

The work is supported by Total and the results are requested to only Total at this time.

D. References

1. Attou, A., Boyer, C. and Ferschneider, G. (1999). Modeling of the Hydrodynamics of the Cocurrent Gas-Liquid Flow in a Trickle-Bed Reactor. *Chemical Engineering Science*, 54, 785-802
2. Attou, A and Ferschneider, G. (2000). A Two-Fluid Model for the Transition between Trickle and Pulse Flow in a Cocurrent Gas-Liquid Packed-Bed Reactor. *Chemical Engineering Science*, 55, 491-511
3. Jiang, Y., Khadilkar, M.R., Al-Dahhan, M.A. and Dudukovic, M.P. (2002). CFD of Multiphase Flow in Packed-Bed Reactors: I. k-Fluid Modeling Issues and II. Results and Applications. *AIChE Journal*, 48, 701-730
4. Kumar, S. B., M. P. Dudukovic, et al. (1997). "Measurement techniques for local and global fluid dynamic quantities in two and three phase systems." *Non-Invasive Monitoring of Multiphase Flows*: 1-45.
5. Kumar, S. B. and M. P. Dudukovic (1997). "Computer assisted gamma and X-

ray tomography: applications to multiphase flow systems." Non-Invasive Monitoring of Multiphase Flows: 47-103.

E. Appendix

Description of the experimental setup

The experimental setup consists of a 14 cm inner diameter Plexiglas column with 3 mm mean diameter glass beads randomly packed into it. Water is introduced through two inlets – a centered single point liquid inlet pipe of 0.7 cm inner diameter or an industrial distributor – in the center on the top of the bed at superficial velocities of 1, 2, 4, 6 and 8 mm.s⁻¹. Air enters the reactor through a separate tube located high enough at 80 cm above the bed to ensure uniform gas distribution on the top surface of the packing and to avoid any disturbance on the liquid inlet flow. Air flows downward, cocurrently with water, at superficial velocities ranging from 0 to 0.8 m.s⁻¹.

I-16. Study of Liquid Spreading From a Point Source in a Trickle Bed Via Gamma-Ray Tomography and CFD Simulation

Introduction

Fixed bed reactors are extensively used in industrial processes. In refining, hydro-treatment processes in general, and hydro-desulfurization in particular, involve two-phase gas-liquid flow through a fixed catalyst bed. Due to the rising environmental constraints, the level of sulfur in both gasoline and diesel are subject to severe restrictions. The improved design of the distributor, of reactor internals and of the bed structure, all aim at achieving improved utilization of the catalyst bed and better reactor performances. For instance, a new gas-liquid distributor and an optimized guard bed structure are developed to provide a homogeneous gas-liquid distribution inside the catalytic bed. The improvement of the contact between the three phases (gas, liquid and catalyst) enhances the transport phenomena and allows better overall reaction yields.

In the past, few studies have been performed to evaluate what is the real impact of catalyst bed structure on the radial spreading of liquid trickling flows. Several experimental investigations have been conducted to monitor the flow pattern of a liquid trickling inside a rectangular column (Lutran *et al.*, 1991, Reinecke and Mewes, 1997, Ravindra *et al.*, 1997, Jiang *et al.*, 1999) or the liquid distribution at the bed outlet (Marcandelli *et al.*, 2000). Reinecke and Mewes (1997) have used capacitance tomography to investigate the two-phase gas-liquid flow inside a trickle bed. Since 2D images of gas-liquid are shown, these images are mainly qualitatively interpreted and it is not possible to deduce liquid flow spreading inside the bed. Ravindra *et al.* (1997) and Jiang (1999) have performed visualization experiments to detect liquid flow inside the bed (by dye absorption measured after bed dismantling) or at the reactor wall with a colored liquid. These studies give interesting results about the liquid flow structure inside the bed, but it is impossible to quantify the liquid retention variations along the bed axis. Lutran *et al.* (1991) performed measurement of liquid retention using X-ray tomography inside a small column with a square section of 6.03 cm width. The effect of particle diameter and bed pre-wetting on liquid distribution have been studied with different fluids. Though there is a good resolution in the images obtained, the data are not interpreted in terms of liquid retention. Further more the interaction between liquid and gas flows is not studied since there is no gas flow rate.

Much effort has been also devoted to develop 2D or 3D models to simulate liquid flow inside a trickle bed (Jiang *et al.*, 2002, Gunjal *et al.*, 2003). Nevertheless, up to now these codes have almost never been validated with experimental results of liquid flow distribution measured over the cross-section of a fixed bed. In the work of Gunjal *et al.* (2003), the CFD results are compared to RTD experimental data but unfortunately these measurements are not very sensitive to liquid maldistribution since different phase distributions can produce the same RTD results.

In the present work, a flow configuration corresponding to the injection of a single liquid jet inside a trickle bed has been tested. The liquid is directly injected at the bed inlet using a single tube and the gas flow is introduced all over the bed cross section. The liquid

distribution over the column cross section is measured using both a gamma ray tomographic system at three different positions along the bed axis (to assess liquid holdup distribution) and a segmented collecting device at the bed outlet (to assess liquid flux distribution).

The experimental data are processed to obtain the liquid spreading angle as a function of particle diameter, liquid and gas flow rate in both a pre-wetted and non pre-wetted bed. These results are then used to evaluate the two-dimensional (2D) computational fluid dynamic model (CFD) developed at the CREL laboratory for gas/liquid trickle flows inside a fixed bed (Jiang et al., 2002). This model is implemented in the CFDLIB code of the Los Alamos Laboratory. Several closure laws reported in the literature for liquid/solid, gas/solid friction forces (Holub et al., 1992), for gas/liquid friction force (Attou et al., 1999) and finally for capillary pressure are used. A new model for capillary pressure has been proposed to correctly predict the liquid radial spreading.

Experimental Study

Experimental setup

The experiments were conducted in a 0.4 m inner diameter column filled with a 1.8 m high bed of spherical particles. The fluids used are water for liquid phase and air for gas phase. The particles are glass beads 1.99 mm in diameter. The bed porosity has been measured at different bed heights and the following profile of cross averaged bed porosity $\varepsilon_0(z)$ has been deduced :

$$\varepsilon_0(z) = 0.0469 z^2 - 0.1242z + 0.4209 \quad (1)$$

The liquid flow is introduced through a single tube with 8 mm inner diameter that is immersed in glass beads 15 mm downstream from the top of the bed. The gas phase is injected all around the liquid tube over the whole bed section on the top.

Table 1 summarizes the selected operating conditions for the three tests performed. Two experiments were conducted with bed initially dried with same liquid flow rate and two different gas flow rates. The third experiment is conducted with bed initially pre-wetted. The pre-wetting consists in using a liquid ascending flow and then bed draining by gravity.

Liquid distribution measurements

The liquid distribution over the bed cross section has been measured using two different ways:

- Measurement of liquid retention (saturation) distribution in the bed cross section using a gamma ray tomographic system. The cross-sectional liquid retention maps are obtained at three different distances from liquid feed tube outlet : 60, 280 and 780 mm. The tomographic system is composed of a Cesium137 source with 300 mCi in activity and 32 detectors with BGO crystals. This system has been largely described in Boyer and Fanget (2002). In the present configuration the 64x64 pixels images are obtained allowing a spatial resolution of 6.25x6.25 mm².
- Measurement of liquid flux distribution at bed outlet using a liquid collecting device. The gas/liquid flow is collected at bed outlet following 25 sectors with same area.

The gas and liquid flows are then separated and the liquid flux is deduced from the liquid height measurement in a transparent tube, these liquid height being established by upstream calibrated orifices.

During the tests, two zones appear inside the bed : one with high liquid retention and one with dry zone with only gas flow. Thus a high density gradient occurred at the boundary of the two zones. In this configuration, the classical reconstruction program using filtered back-projecting algorithm are not the best since the filtering step makes the contours of dense object blurred on reconstructed images. Thus a new algorithm based on algebraic reconstruction has been developed (Koudil et al., 2003). This algorithm is able to take into account zones with density gradients, once a threshold has been defined for the density gradient level. Figure 2 show a comparison of the same image processed by the classical filtered back-projecting algorithm and the algebraic algorithm. One can see that the determination of liquid zone radius from the liquid retention radial profile is more accurate using the new algorithm : the determined radius is 85 mm for the classical algorithm and 72 mm for the new one that corresponds to a discrepancy of 15 %.

Experimental Results

Figure 3 presents both the images of liquid retention corresponding to tomographic measurement at three levels and images of liquid flux at bed outlet for the three tests performed : case 1, 2 and 3 (see table 1). In all cases the liquid flow spreading remains moderate and liquid almost never reach the column wall. It is thus possible to evaluate the liquid jet contour, initial angle and spreading length. The liquid jet radius is deduced from liquid retention radial profile. These profiles are obtained by averaging liquid retention from tomographic measurement over angular position as following :

$$\beta_L(r) = \int_0^{360} \int_{r-\Delta r/2}^{r+\Delta r/2} \beta_L(i, j) dr d\theta \quad (2)$$

where $\beta_L(i, j)$ is the liquid retention inside the bed porosity for pixels (i, j) in the images. β_L correspond to the fraction of bed porosity occupied by liquid phase.

The radial profiles of liquid retention are shown in Figure 4. As one can see, the first profile obtained near liquid injection is continuous and regular and the measured liquid saturation is progressively disturbed due to liquid flow interaction with the bed structure. The observed tendency remains physical, with liquid retention decreasing from the bed axis to “jet” periphery, and it is always possible to detect properly the jet contour. The values of liquid jet radius used for the “jet” contour, spreading angle and length determination are listed in table 2. The spreading length is evaluate by determining the axial evolution of the spreading angle with a fitted linear function. The spreading length corresponds to the axial coordinate where the spreading angle vanishes.

The results show that the spreading angle remains low at values of about 5° for non wetted bed. The initial pre-wetting of bed creates a significant increase of jet spreading angle that is doubled. As expected, the increase of gas flow rate induces to confine liquid jet by increasing gas/liquid shear force at liquid zone periphery. It can also be noted that gas flow rate increase

has a drastic effect on spreading length who is divided by two when gas flow rate is doubled. The gas flow rate increase accelerates the jet establishment by enhancing interactions between gas/liquid flow and fixed bed.

CFD Simulations

In the Eulerian k-fluid approach, different phases are treated as interpenetrating continua. The derivation of the conservation equations for mass, momentum and enthalpy is performed by using either the volume averaging or ensemble averaging technique to describe the time-dependent motion of fluids and track the volume fraction distribution of each phase.

A package, CFDLIB, developed by the Los Alamos National Laboratory (Kashiwa & Rauenzahn; 1994), is used for the transient multiphase flow simulations presented in this paper.

The ensemble-averaged conservation equations that serve as the basis for k-fluid model in CFDLIB are:

Mass balance equation (continuity):

$$\frac{\partial \rho_k}{\partial t} + \nabla \cdot \rho_k \bar{u}_k = \langle \rho_0 \dot{\alpha}_k \rangle \quad (3)$$

Momentum balance equation:

$$\frac{\partial \rho_k \bar{u}_k}{\partial t} + \nabla \cdot \rho_k \bar{u}_k \bar{u}_k = \langle \rho_0 \dot{\alpha}_k \bar{u}_o \rangle - \nabla \cdot \langle \alpha_k \rho_0 \bar{u}_k' \bar{u}_k' \rangle + \langle \alpha_k \nabla p_0 \rangle + \langle \alpha_k \nabla \cdot \bar{\bar{\tau}}_0 \rangle + \rho_k \bar{g} \quad (4)$$

After decomposing the pressure and stress terms in terms of pressure acceleration and material stress divergence, one can get the following momentum equation:

$$\begin{aligned} \frac{\partial \rho_k \bar{u}_k}{\partial t} + \nabla \cdot \rho_k \bar{u}_k \bar{u}_k = & \langle \rho_0 \dot{\alpha}_k \bar{u}_o \rangle - \nabla \cdot \langle \alpha_k \rho_0 \bar{u}_k' \bar{u}_k' \rangle - \theta_k \nabla p - \nabla \theta_k (p_0^k - p) \\ & - \langle [-(p_0 - p) \bar{\bar{I}} + \bar{\bar{\tau}}_0] \cdot \nabla \alpha_k + \nabla \cdot \langle \alpha_k \bar{\bar{\tau}}_0 \rangle + \rho_k \bar{g} \end{aligned} \quad (5)$$

To use Equation (5), the closure models for computing the Reynolds stress, the momentum exchange terms, and the interfacial tension effect are needed.

Closure Laws

Since the fluctuations are dampened by the packing in the trickle bed, the Reynolds stress term can be neglected. Only the momentum exchange term and the interfacial tension effect need to be closed. In this paper, the Single Slit Model (Holub *et al*, 1992) is used to close the fluid-particle momentum exchange term, the Two-Fluid Interaction Model (Attou *et al.*, 1999) is used to close the gas-liquid momentum exchange term.

$$X_{kS} = \left(A_{kS} \mu_k U_k + B_{kS} \rho_\alpha U_k^2 \right) \frac{1}{(1-\varepsilon) |u_k|} \quad (\text{Holub et al., 1992}) \quad (6)$$

$$X_{gl} = \frac{\theta_g}{\varepsilon} \left(A_{gl} \mu_g U_r + B_{gs} \rho_g U_r^2 \right) \frac{1}{(1-\varepsilon) |u_g - u_l|} \quad (\text{Attou et al., 1999}) \quad (7)$$

where

$$A_{kS} = 180 \frac{(1-\varepsilon)^2}{\theta_k^3 d_p^2}; \quad B_{kS} = 1.8 \frac{(1-\varepsilon)}{\theta_k^3 d_p}; \quad A_{gl} = 180 \frac{(1-\theta_g)^2}{\theta_g^3 d_p^2} \left(\frac{1-\varepsilon}{1-\theta_g} \right)^{2/3};$$

$$B_{gl} = 1.8 \frac{(1-\theta_g)}{\theta_g^3 d_p} \left(\frac{1-\varepsilon}{1-\theta_g} \right)^{1/3}; \quad U_r = \theta_g |u_g - u_l|.$$

Jiang et al.'s (2002) implementation approach is used in this paper. The gas-liquid interfacial tension effect can be modeled by either the capillary pressure correlation suggested by Attou and Ferschneider (2000) or Grosser et al. (1988):

$$p_L = p_G - 2\sigma_s (1-f) \left(\frac{\theta_s}{1-\theta_G} \right)^{1/3} \left(\frac{1}{d_p} + \frac{1}{d_{\min}} \right) F \left(\frac{\rho_G}{\rho_L} \right) \quad (\text{Attou and Ferschneider, 2000}) \quad (8a)$$

$$p_L = p_G - (1-f) \sigma_s \frac{\sqrt{180} \theta_s}{(1-\theta_s) d_e} \left[0.48 + 0.036 \ln \left(\frac{1-\theta_s - \theta_L}{\theta_L} \right) \right] \quad (\text{Grosser et al., 1988}) \quad (8b)$$

where the wetting efficiency is given by El-Hisnawi (1981).

$$f = 1.021 \left(\frac{\theta_l}{1-\theta_s} \right)^{0.224} \quad (9)$$

One should note that the gradient of the capillary pressure and liquid volume fraction are important in the momentum source term in equation (5).

It has been shown (Jiang et al., 2002) that k-fluid CFD model predictions, with surface tension effect implemented as illustrated above, are comparable with experimental data (Szady and Sundaresan, 1991) for trickle bed with uniform gas and liquid feeds. However, the single source liquid inlet configuration in this work is significantly different than previous investigation (Jiang et al., 2002), in which the distributed liquid inlet case was considered with the focus on the effect of the bed porosity distribution on both gas and liquid phase flow velocity and retention. In that case all computing cells had small amount of gas and liquid. In the present case of the single source liquid inlet configuration, many cells have either gas-only or liquid-only situation. The objective is to evaluate if the existing system equation is still able to predict radial dispersion of real 2D axi-symmetrical two-phase gas-liquid flow inside a fixed bed. Thus, the main purpose of the simulation performed in this

paper is to examine whether the previously implemented formula (Jiang et al., 2002) can also predict the liquid spreading issuing from a single inlet source. This is a much more challenging task.

Simulation setup

2D axi-symmetric coordinates are used in this paper. The grid size is 1 cm for axial direction, and 0.4 cm for radial direction. Local bed porosity is generated based on Equation (1). No-slip boundary condition is imposed at the wall ($r = 0.2$ m), and the outflow boundary condition (i.e., zero normal gradient) is imposed at bottom of the TBR ($z = 101$ cm). At the top of the TBR, gas is uniformly introduced for $0.4 \text{ cm} < r < 20 \text{ cm}$, and liquid is fed in with range $0 < r < 0.4 \text{ cm}$. The gas/liquid velocity and holdup at the boundary is calculated based on the superficial velocity of each phase and the bed porosity at the top of the TBR. The initial liquid holdup for the non-pre-wetted bed is set to be 0.0, and for the pre-wetted bed is set to be 0.05.

Comparison of CFD Results with Experimental Data

The implementation illustrated above does not take the flow history dependence into account. Thus, the predicted liquid spreading is independent of initial conditions, and is over-predicted as illustrated in Figure 5.

It must be noted, however, that the gradient of capillary pressure in momentum equation (5) has a predominant effect on radial dispersion. To address this shortcoming, we propose the expressions given by Equation (10) to model the surface tension effect for pre-wetted and non-pre-wetted beds in the current configuration (i.e., single source liquid inlet). We know that the capillary pressure (i.e., $p_G - p_L$) should be lower in pre-wetted bed than in the non-pre-wetted bed. To accomplish this we change the dependence of capillary pressure on the wetting efficiency in pre-wetted and non-pre-wetted beds as shown below.

$$p_L = p_G - 2\sigma_s (1-f)^{-0.2} \left(\frac{\theta_s}{1-\theta_G} \right)^{1/3} \left(\frac{1}{d_p} + \frac{1}{d_{\min}} \right) F \left(\frac{\rho_G}{\rho_L} \right) \quad (\text{Pre-wetted}) \quad (10a)$$

$$p_L = p_G - 2\sigma_s (1-f)^{-0.6} \left(\frac{\theta_s}{1-\theta_G} \right)^{1/3} \left(\frac{1}{d_p} + \frac{1}{d_{\min}} \right) F \left(\frac{\rho_G}{\rho_L} \right) \quad (\text{Non-pre-wetted}) \quad (10b)$$

While this provides the correct trends of experimental results, the physics behind it remains to be explained. The inter dependence of capillary pressure term and wetting efficiency is still to be cleared. The force that appears at contact angle between gas, liquid and solid in non wetted has to be taken into account by some means or other.

The model predictions for the liquid retention spreading for Case 1, 2, and 3 are illustrated in Figure 6. It must be noted that liquid retention calculated by CFD code (named THE2) corresponds to fraction of total reactor volume occupied by liquid. The experimental contour of jet presented on left hand side is deduced from measured jet radius (see table 2). The

implementation qualitatively predicts the trend of liquid spreading in all cases. Liquid spreads more in per-wetted bed, and liquid spreading is reduced when gas flow rate increases. However, the model under-predicts the liquid spreading in non-pre-wetted bed, while over-predicts the liquid spreading in pre-wetted bed, which indicates that the power factor on $(1-f)$ needs to be adjusted. This points out the need for a more detailed model based on DNS at the point of liquid injection.

Conclusions

The computed tomography (CT) has been implemented at IFP to detect the evolution of the liquid cross-sectional saturation profiles as one moves downstream from a single point liquid injector. The CT can quantify the liquid spreading in pre-wetted and non-pre-wetted beds for different gas and liquid flow rates.

Euler-Euler simulation can semi-quantitatively predict the liquid spreading from a point source but relies on empirical closures as for instance capillary pressure which need further adjustment and study.

The single source liquid inlet configuration in this work is significantly different than previous investigation (Jiang et al., 2002), in which the distributed liquid inlet was considered with the focus on implementation of porosity distribution and assessment of its effect on liquid and gas flow and saturation map. In the present study the CFD code has to be able to handle a real 2D tow phase flow configuration inside a trickle bed with high liquid retention gradient (many cells have either gas-only or liquid-only situation).

The implementation of capillary pressure (Jiang et al., 2002), with modification proposed in this paper to account for bed initial wetting condition and very low gas holdup and very low liquid holdup in some cells, can qualitatively predict the trend of liquid spreading from a single source liquid inlet. The results show the predominant effect of this closure law on liquid radial spreading inside the bed. The proposed modification needs further adjustment to fit the experimental data better. In addition, the proposed adjustment needs to be tested and against distributed liquid inlet case (not necessary uniform) and against different bed geometry (particles diameter) or fluid properties (surface tension and contact angle). Improved physical understanding is also needed.

Acknowledgement

The authors would like to thank fruitful discussion with Dr. Jiang and Dr. Ferschneider.

Nomenclature

d_{\min} Minimum equivalent diameter of the area between three spheres in contact
 $(d_{\min} = \left(\frac{\sqrt{3}}{\pi} - 0.5 \right)^{0.5} d_p), \text{ m}$

d_p	Particle diameter, m
f	Particle wetting factor, dimensionless
$F\left(\frac{\rho_G}{\rho_L}\right)$	Pressure factor, $\left(F\left(\frac{\rho_G}{\rho_L}\right) = 1 + 88.1 \frac{\rho_G}{\rho_L}\right)$, dimensionless
p	Pressure, Pa
t	Time, s
U	Superficial velocity, m/s
X_{kl}	Momentum exchange coefficient between phase k and phase l, $\text{kg m}^{-3} \text{s}^{-1}$
z	Axial coordinate, m

Greek Symbols

β_l	Liquid retention (saturation), dimensionless
ε	Bed local porosity, dimensionless
ε_0	Cross averaged bed porosity, dimensionless
θ	Phase holdup, dimensionless
ρ	Density, kg m^{-3}
σ_s	Surface tension, N/m

Subscript

g	Gas index
k	Phase index
l	Liquid index
s	Solids index

REFERENCES

1. Attou, A., Boyer, C. and Ferschneider, G. (1999), Modeling of the hydrodynamics of the cocurrent gas-liquid trickle flow through a trickle bed reactor, *Chem. Eng. Science*, **54**, 785-802
2. Attou, A. and Ferschneider, G. (2000), A two-fluid hydrodynamic model for the transition between trickle and pulse flow in a cocurrent gas-liquid packed bed reactor, *Chem. Eng. Sci.*, **55**, 491-511.
3. Boyer, C. and Fanget B. (2002) Measurement of Liquid Flow Distribution in Trickle Bed Reactor of Large Diameter with a New Gamma-ray Tomographic System, *Chem. Eng. Sci.*, **57**, 1079-1089.
4. El-Hisnawi, A. A. (1981). Tracer and reaction studies in trickle-bed reactors. D.Sc. Thesis, Washington University, St. Louis, USA.
5. Jiang, Y., Khadilkar, M. R., Al-Dahhan, M. H., Dudukovic, M. P. (1999) Two-phase flow distribution in 2D trickle bed-reactors, *Chem. Eng. Science*, **54**, 2409-2419.
6. Jiang, Y., Khadilkar, M.R., Al-Dahhan, M.A. and Dudukovic, M.P. (2002). CFD of Multiphase Flow in Packed-Bed Reactors: I. k-Fluid Modeling Issues and II. Results and Applications. *AIChE Journal*, **48**, 701-730

7. Kashiwa, B. A. and Rauenzahn, R. M. (1994). A multimaterial formalism. FED (Am. Soc. Mech. Eng.), 185, 149-157.
8. Kantzas A. (1994), Computations oh holdups in fluidized and trickle beds by computer-assisted tomography, *AIChE J.*, 40, 1254.
9. Koudil, A., Boyer, C. and Bentolila, Y. (2003), Measuring of liquid and gas flow distribution in a fixed bed reactor using a gamma-ray tomographic system, Proceeding of 3rd World Congress On Industrial Process Tomography, 2-5 sept 2003, Banff, Canada.
10. Holub, R.A., Dudukovic, M.P., and Ramachadran, P.A. (1992) A phenomenological model for pressure drop, liquid holdup, and flow regime transition in gas-liquid trickle flow, *Chem. Eng. Sci.*, 47, 2343-2348.
11. Lutran, P.G., Ng, K.M. and Delikat, E.P. (1991), Liquid distribution in trickle beds. An experimental study using computer-assisted tomography, *Ind. Engng. Chem. Res.*, 30, 951.
12. Marcandelli, C.; Lamine, A.S.; Bernard, J.R.; Wild, G., 2000, Liquid distribution in trickle-bed reactor, *Oil & Gas Science and Technology*, 55, 407-415.
13. Gunjal, P.R., Ranade, V.V., Chaudhari, R.V., 2003, Liquid distribution and RTD in trickle bed reactors : experiments and CFD simulations, *The Can. J. of Chem. Eng.*, 81,3-4, 821-830
14. Grosser, K. A., Carbonell, R. G. and Sundaresan, S. (1988) Onset of pulsing in two-phase cocurrent downflow through a packed bed. *A.I.Ch.E. J.*, 34, 1850.
15. Ravindra, P.V., Rao, D.P. and Rao, M.S. (1997), Liquid flow texture in Trickle-Bed Reactors : an experimental study, *Ind. Eng. Chem. Res.*, 36, 5133-5145
16. Reinecke, N. and Mewes, D. (1997), Investigation of the two-phase flow in trickle-bed reactors using capacitance tomography, *Chem. Eng. Science*, 52, 2111-2127.
17. Szady, M. J. and Sundaresan, S. (1991) Effect of boundaries on trickle-bed hydrodynamics, *A.I.Ch.E. J.*, 37, 1237-1241.

Table 1 : Operating conditions for the tests

Case	Liquid flow rate (L/h)	Gas flow rate (m ³ /h)	Bed pre-wetting
1	128	45	No
2	128	90	No
3	128	45	Yes

Table 2 : Characteristics of liquid jet measurements from tomographic images.

Case	1	2	3
Q_L (L/h)	128	128	128
Q_G (m³/h)	45	90	45
Pre-wetting	no	no	yes
R_{jet} (mm) à -60 mm	52	52	60
R_{jet} (mm) à -280 mm	72	70	103
R_{jet} (mm) à -780 mm	94	62	160
Jet spreading angle (°)	5.2	4.7	11.1
Spreading length (mm)	488	244	

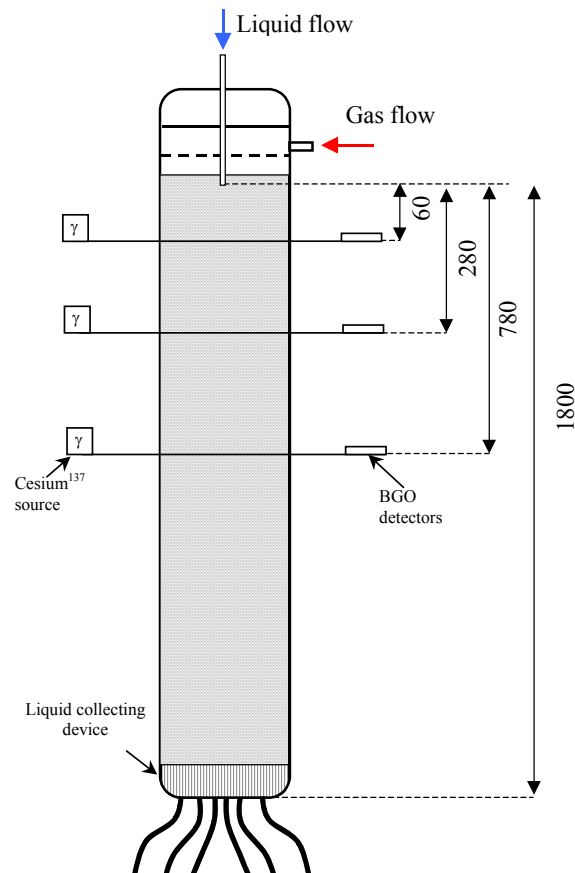


Figure 1 : Schematic of experimental setup

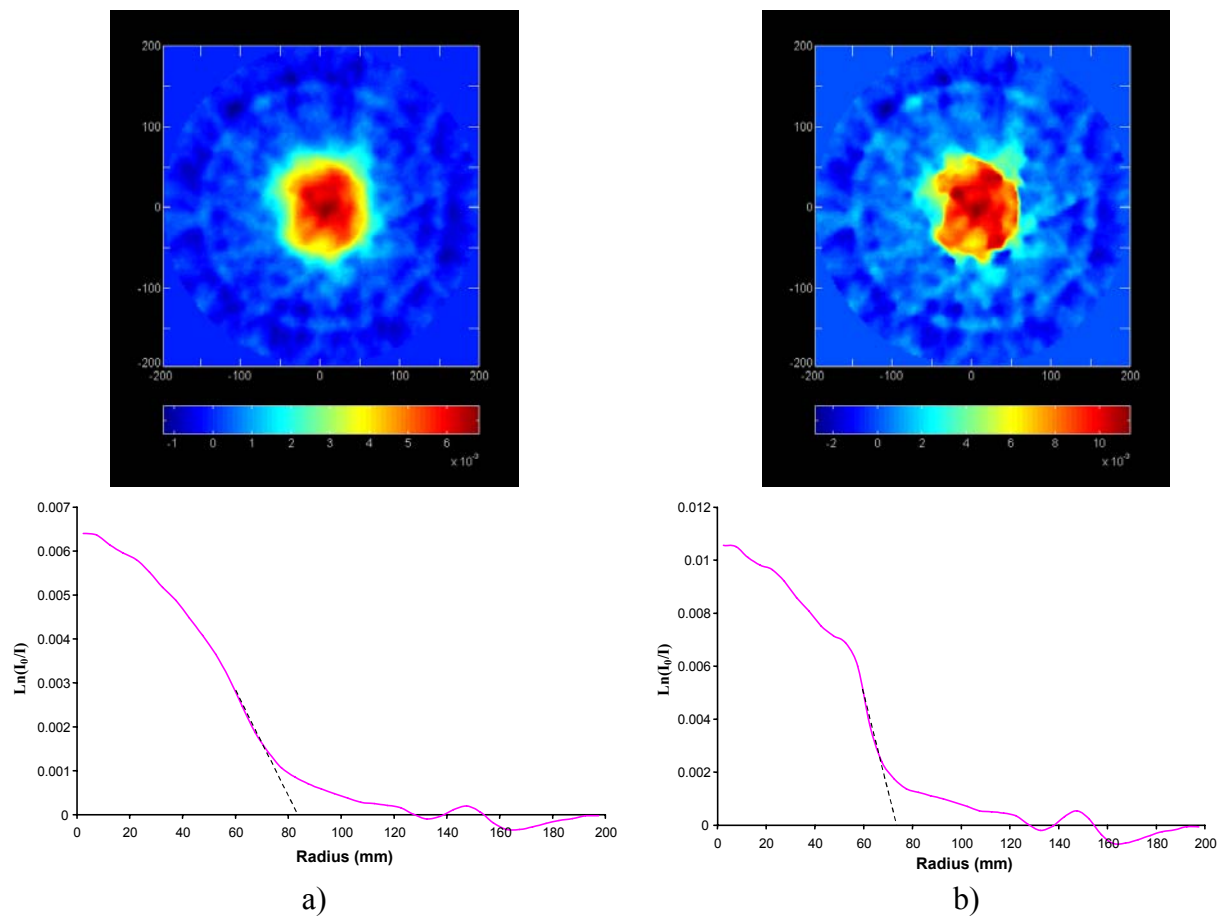


Figure 2 : Comparison of images reconstructed with : a) classical filtered back-projecting algorithm, b) algebraic reconstruction algorithm.

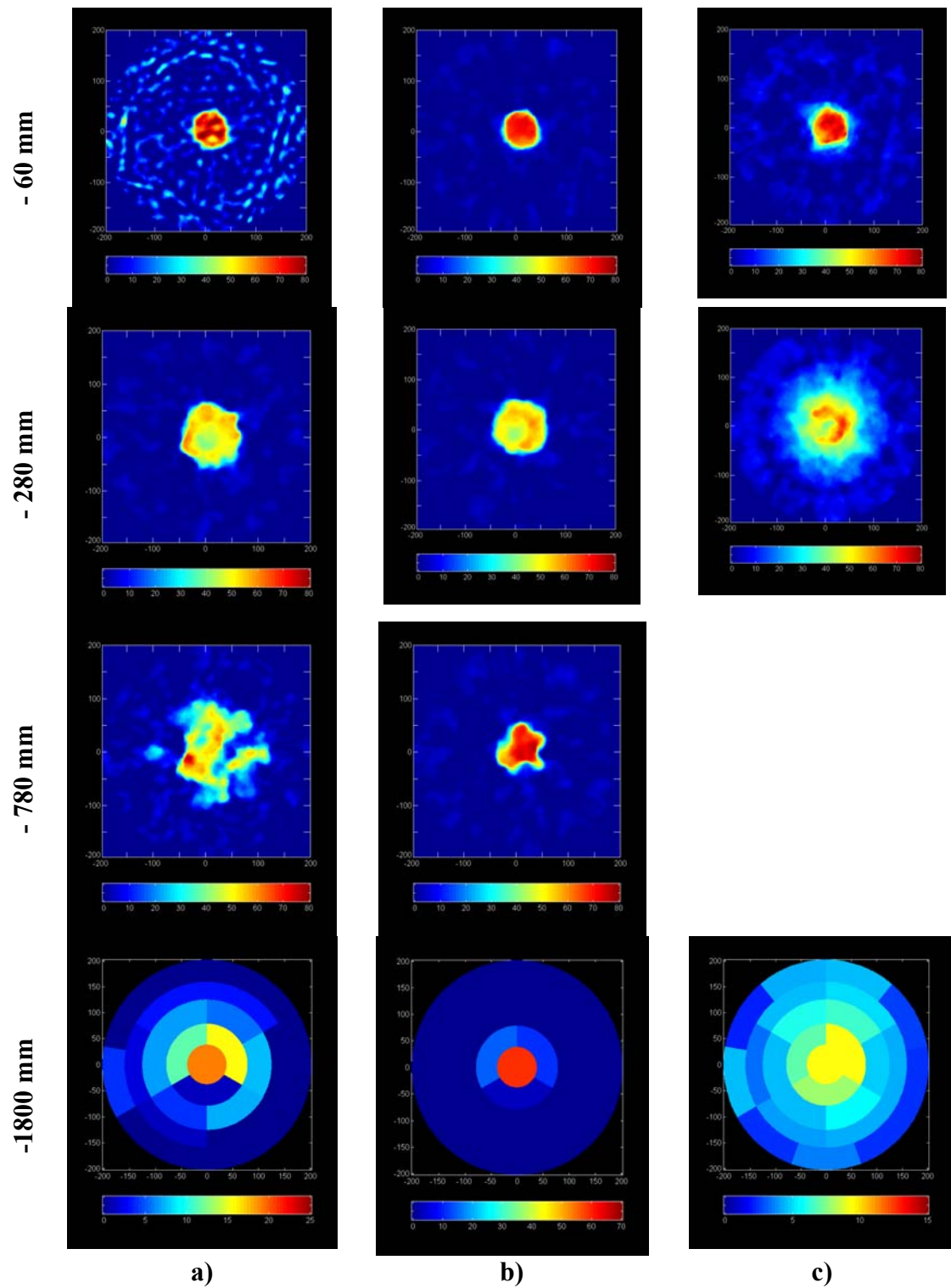
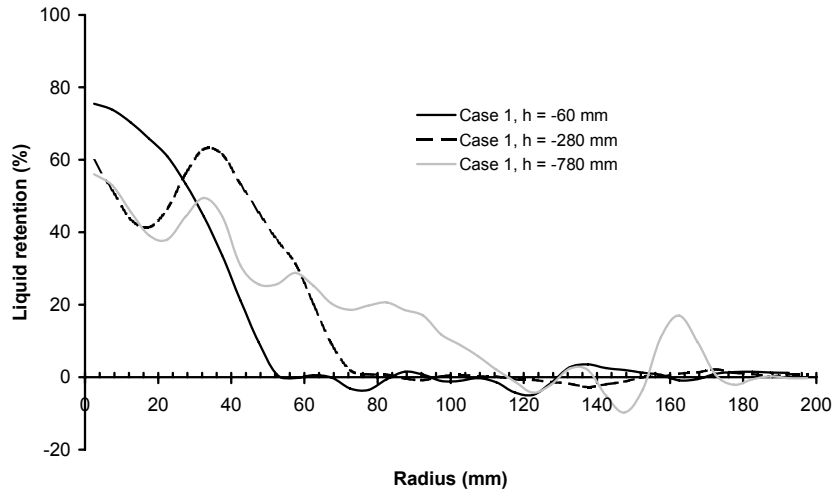
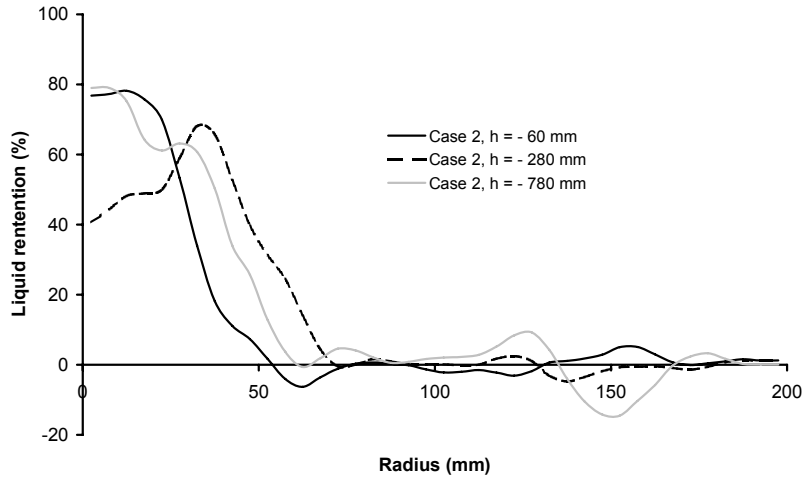


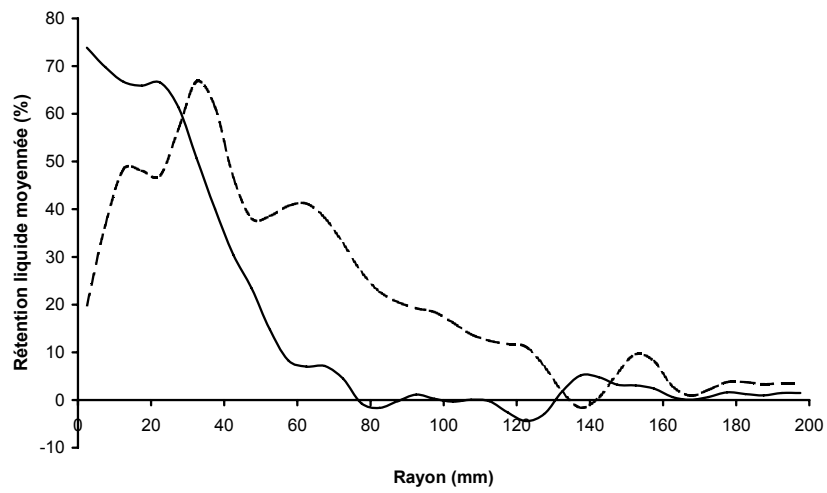
Figure 3 : Images of liquid retention (saturation) (top three rows) and liquid flux distribution (bottom row) over the column cross section at different bed levels for : a) case 1, b) case 2, c) case 3.



a)



b)



c)

Figure 4 : Measured liquid retention (saturation) profiles for different levels inside the bed :
 a) Case 1, b) case 2, c) case 3.

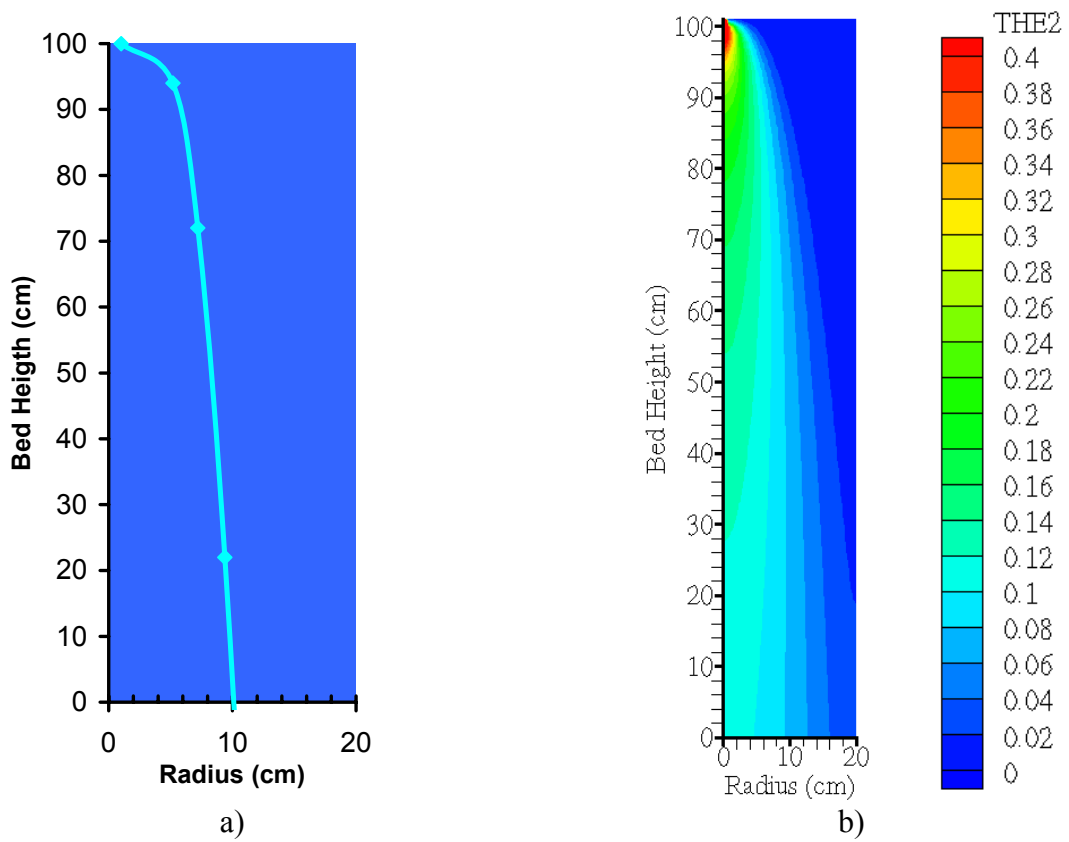
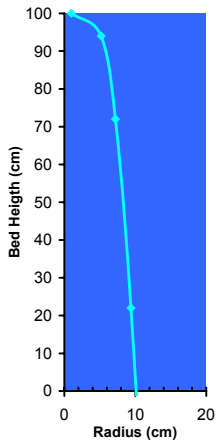
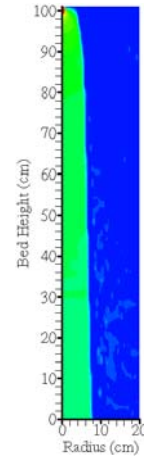


Figure 5 : Comparison of experimental results for liquid holdup and liquid jet contour deduced from experimental data for case 1 : a) experimental jet contour, b) CFD simulation.

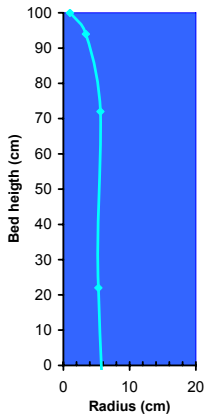


Experimental liquid zone contour

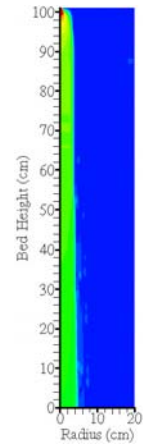


CFD Simulation

a)

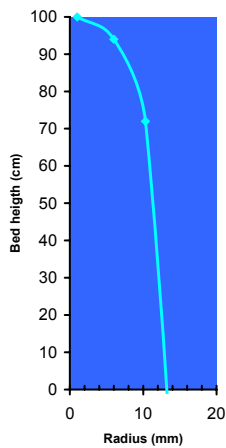


Experimental liquid zone contour

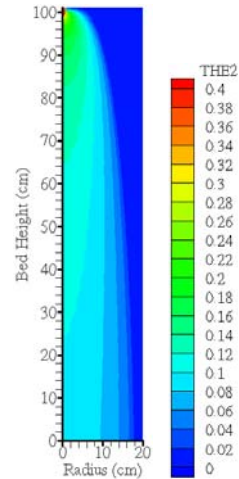


CFD Simulation

b)



Experimental liquid zone contour



CFD Simulation

Figure 6 : Comparison of CFD simulation results for 2D axisymmetric liquid holdup and liquid jet contour deduced from experimental data : a) case 1, b) case 2 and c) case 3.

